Climatic Change (2012) 115:709–724
DOI 10.1007/s10584-012-0462-0

The effects of rerouting aircraft around the arctic circle on arctic and global climate

Mark Z. Jacobson · Jordan T. Wilkerson · Sathya Balasubramanian · Wayne W. Cooper Jr. · Nina Mohleji

Received: 10 November 2011 / Accepted: 23 March 2012 / Published online: 13 April 2012

Abstract Climate data suggest greater warming over the Arctic than lower latitudes, and the most abundant direct source of black carbon and other climate-relevant pollutants over the Arctic is cross-polar flights by international aviation. A relevant question is whether rerouting cross-polar flights to circumnavigate the Arctic Circle reduces or enhances such warming. To study this issue, a model accounting for subgrid exhaust plumes from each individual commercial flight worldwide was used with 2006 global aircraft emission inventories that treated cross-polar flights and flights rerouted around the Arctic Circle (66.56083 °N), respectively. Rerouting increased fuel use by 0.056 % in the global average, mostly right outside the Arctic Circle, but most of the associated black carbon and other emissions were removed faster because they were now over latitudes of greater precipitation and lesser stability. Rerouting also reduced fuel use and emissions within the Arctic Circle by 83 % and delayed pollutant transport to the Arctic. The Arctic reduction in pollutants, particularly of black carbon, decreased Arctic and global temperature and increased Arctic sea ice over 22 years. Although the slight increase in total CO_2 emissions due to rerouting may dampen the benefit of rerouting over more decades, rerouting or even partial rerouting (allowing cross-polar flights during polar night only) may delay the elimination of Arctic sea ice, which will otherwise likely occur within the next 2–3 decades due to global warming in general. Rerouting may increase worldwide fuel plus operational costs by only ~$99 million/yr, 47–55 times less than an estimated 2025 U.S.-alone cost savings due to the global warming reduction from rerouting.

M. Z. Jacobson (✉) · J. T. Wilkerson
Department of Civil and Environmental Engineering, Stanford University, Stanford, CA, USA
e-mail: jacobson@stanford.edu

S. Balasubramanian
Volpe National Transportation Systems Center, Cambridge, MA, USA

W. W. Cooper Jr. · N. Mohleji
MITRE Corporation Center for Advanced Aviation System Development (CAASD), McLean, VA, USA

1 Introduction

Arctic sea ice has been diminishing since the 1950s (Vinnikov et al. 1999). The minimum annual sea ice extent in 2011 was 2.38±0.05 million square kilometers below the 1979–2000 minimum and close to the lowest minimum ever measured, in 2007 (NSIDC 2011). The reduction in sea ice uncovers the low-albedo Arctic Ocean surface below, accelerating global warming in a positive feedback loop. Above a certain temperature, a tipping point may occur, accelerating the sea ice loss to complete elimination (e.g., Winton 2006), possibly by 2040 (e.g., Holland et al. 2006). Once the ice is completely gone, regenerating the ice may be difficult if the Arctic Ocean reaches a new stable equilibrium (Winton 2006). A permanent loss of the ice may trigger a faster warming feedback of globally averaged temperatures, as solar radiation will then directly warm water over the Arctic Circle, whereas with ice, most such radiation will be reflected.

Arctic air temperatures are sensitive to the presence of anthropogenic pollution. Local sources of such pollution include ice-breaking ships, the ships that follow them, and nearby ships (e.g., Corbett et al. 2010). Surface-emitted pollutants are also transported long distances to the Arctic Circle (66.56083 °N) (e.g., Rahn and McCaffrey 1980; Koch and Hansen 2005; Hegg et al. 2009; Liu et al. 2011; Matsui et al. 2011).

Persistent sources of pollution to the Arctic are cross-polar flights by international commercial aviation. Cross-polar commercial flights became routine starting in 1998, following the Cold War, when the Russian government gave permission for flights across their airspace. Since then, the number of cross-polar flights has gradually increased. Figure 1a shows the total estimated number of cross-polar flights between 2004 and 2010, and Fig. 1b shows the number of cross-polar flights by origin–destination (O-D) market for the same period. The overall growth in number of flights between 2004 and 2010 was 32.1 %, with the peak number occurring in 2008. The total number of O-D markets with cross-polar traffic also increased between 2004 and 2010, from 224 to 278. The largest markets were from Europe to North America, North America to Asia, and North America to Europe, respectively. Cross-polar traffic is expected to grow further with increasing world trade and tourism.

Of the total commercial aviation fuel used worldwide in 2006, about 0.742 % was over the Arctic Circle. However, about 74 % of aircraft emissions within the Arctic Circle were in the stratosphere (Whitt et al. 2011). Since the stratosphere is stable, transport times of pollutants to the surface are high. For example, an inert pollutant emitted at 11 km over the Arctic requires ~70 days in January and ~40 days in July for 50 % of it to reach the

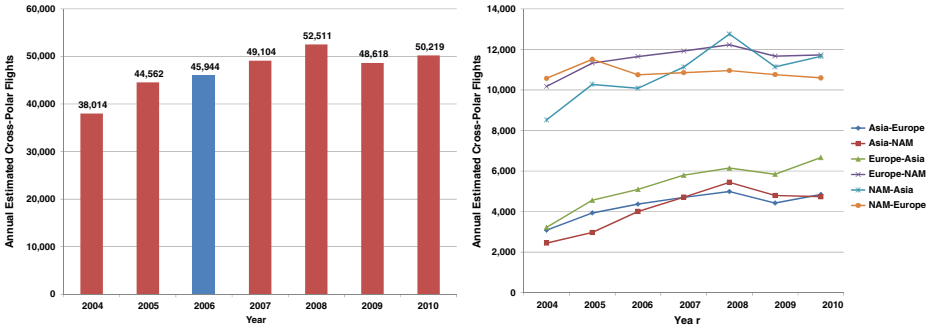

Fig. 1 **a** Estimated number of cross-polar flights 2004–2010. **b** Number of cross-polar flights 2004–2010 by origin–destination region. Flight schedule data were from Innovata, LLC

surface (Whitt et al. 2011). In addition wet removal does not occur until pollutants reach the troposphere Thus, aircraft emissions over the Arctic are long lived and can impact climate there over periods longer than pollutants emitted at lower latitudes or altitudes. Particles emitted at the surface, which are lost primarily by wet deposition, have an *e*-folding lifetime of ~4.5 days averaged globally (Jacobson 2010) but longer over the Arctic than in the global average due to lower precipitation rates over the Arctic.

A relevant question is the consequence of rerouting cross-polar flights to circumnavigate the Arctic Circle. To study this issue, 2006 emission inventories accounting for each individual commercial flight worldwide were developed, one with cross-polar flights and a second with most such flights rerouted around the Arctic Circle. Simulations with a global model that treats exhaust from each individual flight plume independently were then performed to examine the impact of rerouting on climate.

2 Climate model description

The model used for this study, GATOR-GCMOM, is described and evaluated with respect to aircraft-relevant parameters in Jacobson et al. (2011) and Whitt et al. (2011) and with respect to climate response in Jacobson (2010). Briefly, it is a one-way nested global-through-local Gas, Aerosol, Transport, Radiation, General Circulation, Mesoscale, and Ocean Model that simulates climate, weather, and air pollution. It treats emissions; gas photochemistry; size- and composition-resolved aerosol and hydrometeor microphysics and chemistry; size- and composition-resolved aerosol-hydrometeor interactions; subgrid cumulus cloud thermodynamics; grid-scale stratiform thermodynamics; spectral radiative transfer for heating rates and photolysis; dynamical meteorology; 2-D ocean dynamics; 3-D ocean diffusion; 3-D ocean chemistry; ocean–atmosphere exchange; and ice, snow, land surface processes, and subgrid contrail formation and aerosol evolution from each individual flight worldwide.

The model grid scale horizontal resolution was 4°-SN × 5°-WE, with 58 vertical layers up to 0.219 hPa (≈60 km), including 15 in the bottom kilometer, 500-m resolution from 1 to 13 km, and 1-km resolution from 13 to 21 km. The vertical resolution was high in the region of aircraft flights, below 41,000 ft (12.5 km), relative to previous global simulations.

At the grid scale, two discrete (multiple size bin) aerosol size distributions and three discrete hydrometeor distribution, each with multiple components per bin, were used (Jacobson 2010). The two aerosol distributions were an emitted fossil-fuel soot (EFFS) distribution and an internally-mixed (IM) distribution, each with 14 size bins. The three hydrometeor distributions of 30 size bins each were for liquid, ice, and graupel. Each size bin of the EFFS distribution could contain black carbon (BC), primary organic matter (POM), secondary organic matter (SOM), hydrated liquid water, H_2SO_4(aq), HSO_4^-, SO_4^{2-}, NO_3^-, Cl^-, H^+, NH_4^+, NH_4NO_3(s), and $(NH_4)_2SO_4$(s). Each size bin of the IM distribution could contain the same components plus soil dust, pollen, spores, bacteria, and Na^+ (which was a surrogate for Na^+ and the mole equivalent of K^+, Ca^{2+}, and Mg^{2+}). Each size bin of each hydrometeor distribution could contain the same components as in the IM aerosol distribution plus condensed liquid water or deposited ice. Discrete size-resolved EFFS and IM aerosol particles and liquid, ice, and graupel hydrometeor particles and their components could coagulate among each other. Thus, grid-scale aerosol particles and their components were tracked within hydrometeor particles through cloud formation and precipitation.

BC absorption in clouds was treated with the dynamic effective medium approximation (DEMA), which accounted for BC aggregates distributed randomly throughout each hydrometeor particle, as described in Jacobson (2010). Gases, such as HNO_3, HCl, NH_3, H_2SO_4, and organic gases could condense onto or dissolve into grid-scale EFFS and IM aerosol

particles. Liquid water could also hydrate to soluble species and ions could crystallize to solid within such particles. EFFS and IM aerosol particles served as nuclei for new hydrometeor particles. In sum, the model treated indirect, semi-direct, and cloud absorption effects of aerosols on contrails and all other cloud types (Jacobson 2010).

With respect to aircraft, the model simulated the microphysical evolution and optical properties of exhaust plumes and contrails from each individual commercial aircraft flight worldwide at the subgrid scale (their actual size), as described in Jacobson et al. (2011) and Naiman et al. (2010). Size-resolved particle components (BC, POM, S(VI)=H_2SO_4(aq) +HSO_4^-+SO_4^{2-}) and water vapor were emitted from aircraft into subgrid plumes. Size- and composition-resolved contrail particles formed and grew onto the aerosol particles by nucleation, deposition, and coagulation. CO, CO_2, SO_2, NO_x, and speciated total hydrocarbons (THCs) from aircraft were emitted directly to the grid scale. When contrails in subgrid plumes dissipated due to plume expansion and dilution and ice sublimation, water vapor and size- and composition-resolved aerosol cores containing BC, POM, and S(VI) from them were released to the grid scale in the EFFS aerosol distribution, where they affected clouds and radiation. The grid-scale EFFS distribution also contained emissions from other fossil-fuel sources.

3 Baseline and rerouting aircraft emission inventories

The baseline 2006 emission inventory used was developed by the Volpe National Transportation Systems Center and included original flight track emissions from each of 31.3 million commercial flights worldwide (Wilkerson et al. 2010). MITRE Corporation and Volpe developed the rerouting inventory (Cooper et al. 2011; Senzig et al. 2010). The flights chosen for rerouting satisfied the following criteria: (1) they had a filed route above the Arctic Circle, (2) both origin and destination airports were below the Arctic Circle, (c) more than one percent of flights in the origin–destination (O-D) market were cross-polar flights (to remove anomalous flights), (d) they had a great-circle route >500 nautical miles, and (e) they had more than 50 seats (to remove general aviation flights). Thus, short flights, flights with an origin or destination airport within the Arctic Circle, and general-aviation flights were not rerouted.

Based on this analysis, 263 O-D markets had at least one percent of their flights meeting the criteria above in 2006. The number of flights between each origin and destination in these markets was 82,602. Of these, 40,399 (or 0.129 % of all 2006 worldwide commercial flights) were cross-polar. The remaining 42,203 were circumpolar (flying around the Arctic Circle). The number of 2006 cross-polar flights meeting the criteria here (40,399) is less than the number of 2006 cross-polar flights from Fig. 1 because the source of flight inventory data for Fig. 1 (flight schedule data from Innovata, LLC) differed from that of the Volpe baseline inventory developed here for 2006 (Wilkerson et al. 2010). A geographical clustering approach was used to estimate the cross-polar traffic for Fig. 1. That approach assumed that an O-D market had cross-polar traffic if nearby O-D markets with similar great-circle routes had cross-polar traffic based on the MITRE/Volpe rerouting analysis described in this section. This resulted in some additional O-D markets having cross-polar traffic compared with the MITRE/Volpe analysis, which assumed circumpolar routes for those flights due to a complex set of operational rules. The analysis in Fig. 1 allowed for a quick estimate of the cross-polar traffic trends by year.

Next, changes each cross-polar flight's trajectory were simulated. A flight route is a series of 2-D (latitude, longitude) geographical waypoints over which a flight must pass from its origin to destination. The pilot or flight dispatcher files this route with the air traffic control service provider (e.g., the Federal Aviation Administration in the U.S.) prior to departure.

Table 1 2006 change in airborne time and ground distance due to rerouting by flight direction from origin to destination

	East	West	Total
Number of flights	11,453	28,946	40,399
Average reroute minus baseline airborne time (min) (%)	11.01 (+1.85)	19.12 (+2.92)	16.82 (+2.64)
Average reroute minus baseline ground distance (nm) (%)	133.3 (+2.73)	40.74 (+0.79)	66.99 (+1.32)

nm nautical miles

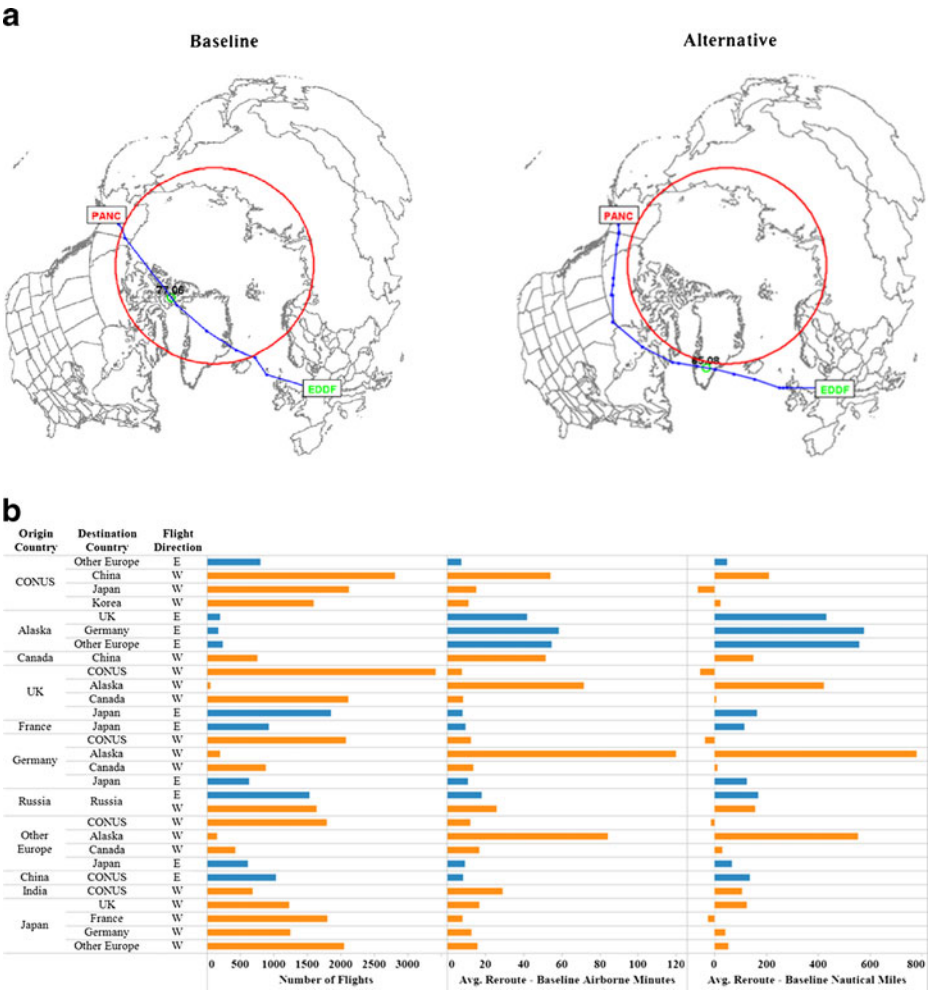

Fig. 2 **a** Baseline (*left*) and selected rerouting (*right*) path of a specific flight from Frankfurt (EDDF) to Anchorage (PANC). **b** Change in airborne time and ground distance due to rerouting flights by origin from regions with more than 400 flights in 2006. *CONUS* Continental United States; *nm* nautical miles

Table 2 Monthly and annual global and Arctic fuel use during 2006 from the baseline and rerouting emission inventories (Tg-fuel). Arctic emissions are those above the Arctic Circle

Month	Base global	Reroute global	% Diff.	Base Arctic	Reroute Arctic	% Diff.
Jan	14.94	14.95	+0.061	0.1068	0.01847	−82.7
Feb	13.58	13.59	+0.066	0.09849	0.01674	−83.0
Mar	15.32	15.34	+0.053	0.1084	0.0197	−82.1
Apr	15.23	15.24	+0.065	0.1140	0.0181	−84.1
May	15.82	15.83	+0.050	0.1176	0.0196	−83.4
Jun	15.90	15.91	+0.048	0.1211	0.0218	−82.0
Jul	16.96	16.97	+0.054	0.1262	0.0239	−82.2
Aug	17.12	17.13	+0.044	0.1311	0.0235	−82.1
Sep	16.05	16.06	+0.052	0.1253	0.0220	−82.4
Oct	16.16	16.17	+0.067	0.1280	0.0211	−83.5
Nov	15.19	15.20	+0.071	0.1098	0.0199	−81.9
Dec	15.80	15.81	+0.046	0.1095	0.0207	−81.1
Year	188.105	188.21	+0.056	1.396	0.244	−82.6

Flight routes are typically planned to minimize airborne time and fuel use by combining wind forecasts with planned cruise altitude and speed information.

Each selected flight taking off or landing in the U.S., Canada, or the U.K. was matched with its planned flight route, obtained from the Enhanced Traffic Management System (ETMS). Flight routes for remaining selected flights, mainly between Europe and Asia, were approximated from available information. Each flight's planned route was used to identify cross-polar and circumpolar flights. For the 40,399 cross-polar flights identified, the path used was the baseline route, and a range of circumpolar reroutes was selected from the 42,203 circumpolar flights among the 263 O-D pairs considered.

The CAASD Analysis Platform for En Route (CAPER) was then used to simulate the 4-D (latitude, longitude, altitude, time) flight path of each baseline and proposed alternative circumpolar routes. The reroute path with the lowest simulated airborne time from origin to destination based on the forecasted winds for that day was chosen for each flight. Some simplifying assumptions were made. First, rerouting was assumed to result in no extra refueling stops or changes to longer-range aircraft to reduce the need for refueling stops. Second, U.S. altitude assignment rules were assumed throughout each flight, even in non-U.S. airspace. Finally, inputs to the model, including aircraft type, were largely derived from historical data, Inputs, such as the planned cruise speed and altitude, were based on aircraft categories, such as a Boeing 747, whereas inputs derived from the Eurocontrol Base of Aircraft Data (BADA) were based on aircraft types, such as a Boeing 747–400.

Each flight's 4-D trajectory was determined as follows. Long distance flights often cannot reach their final cruise altitude until they have burned enough fuel to lighten the aircraft. The flight "steps" from one altitude to the next as it burns more fuel through each interim cruise altitude until it reaches its final cruise altitude, where it maximizes fuel efficiency. Each flight's initial cruise altitude and approximate time needed at each interim cruise level were obtained

Fig. 3 Maps of CO_2-C (kg/m^2) emissions from the baseline and rerouting inventories: **a** global baseline map (162.17 Tg-C; 317.94 mg-C/m^2, **b** global rerouting map (162.26 Tg-C; 318.12 mg-C/m^2), **c** Arctic baseline map (1.204 Tg-C; 56.69 mg-C/m^2), and **d** Arctic rerouting map (0.210 Tg-C; 9.909 mg-C/m^2) ▶

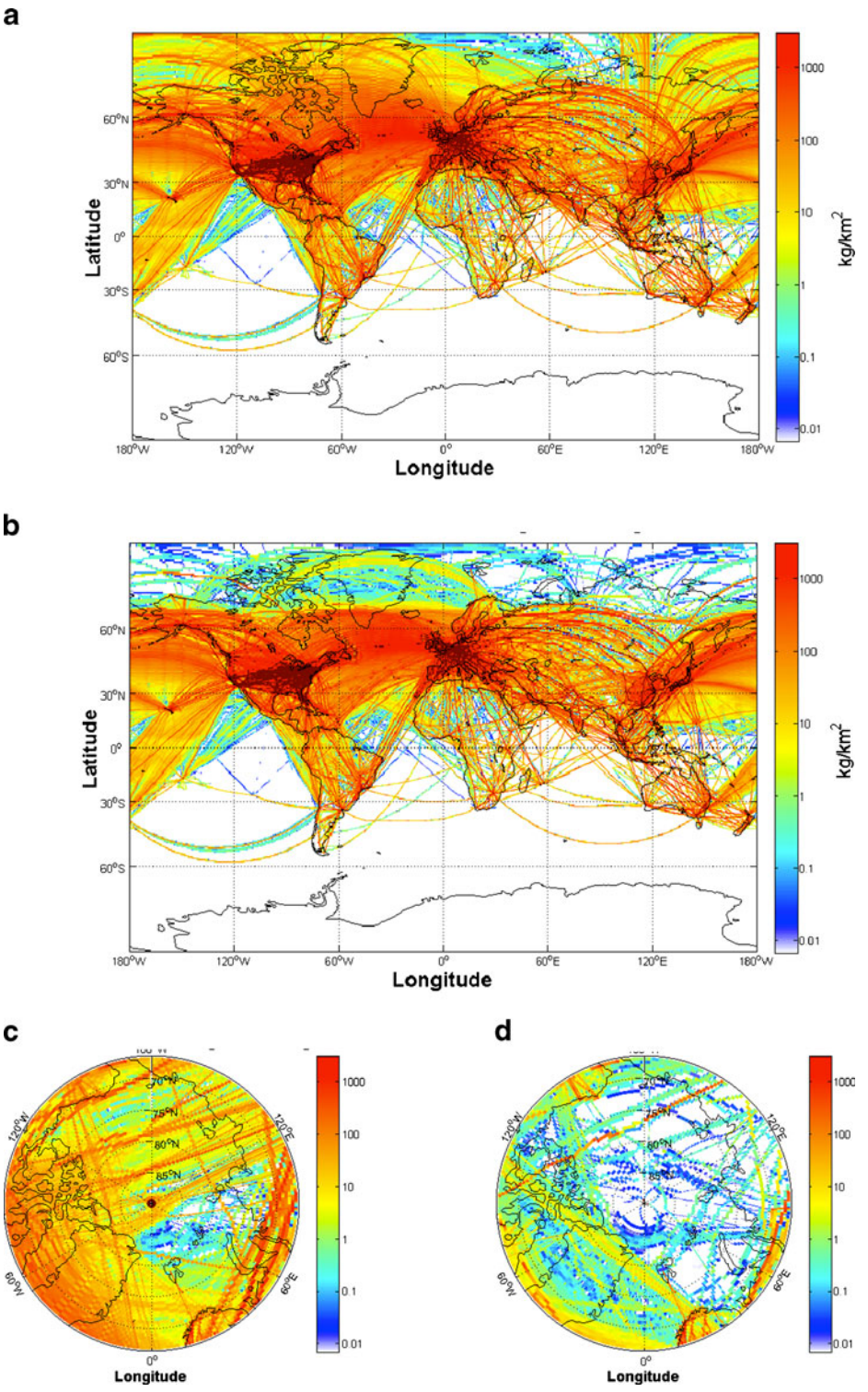
a
Latitude
Longitude
kg/km2
b
Latitude
Longitude
kg/km2
c
Longitude
d
Longitude

from BADA data for each aircraft type. The planned cruise altitude used for each aircraft type was the 75th percentile of the historically filed cruise altitudes for that type. Each flight was assumed to depart at its rated maximum takeoff weight and to fly at its aircraft class's cruise speed corresponding to the current altitude. The planned cruise speed was taken as the average air speed for that aircraft class. Eastbound flights cruise at odd multiples of 1000 ft, and westbound flights cruise at even multiples of 1000 ft. Daily worldwide wind, pressure and temperature reanalysis data at 2.5 °×2.5 ° horizontal resolution and with 17 vertical layers (NCEP/NCAR 2009) were used for the flight trajectory simulations.

Table 1 summarizes the changes in airborne time and ground distances between the average rerouting (circumpolar) trajectories and the baseline (cross-polar) trajectories based on the procedure described here. On average, airborne times for rerouted westbound flights increased by 2.92 %, but those for eastbound times increased by only 1.85 % since eastbound flights are aided by strong westerly tailwinds. Conversely, the change in ground distance for eastbound flights was almost 2 % greater than the change for westbound flights. Thus, the airborne time increase for westbound flights exceeded that for eastbound flights, although the ground distances flown increased more for eastbound flights. This was due to greater headwinds from the prevailing high-altitude westerly (eastbound) Polar jet stream, which slowed westbound flights without changing distance travelled.

Figure 2a illustrates the rerouting of one cross-polar, westbound flight from Frankfurt to Anchorage (EDDF-PANC) to a circumpolar, westbound flight. Rerouting increased the travel distance and exposure to westerly jet stream headwinds, lengthening the flight. EDDF-PANC is the O-D market in 2006 with the largest average simulated increase in both ground distance and airborne time.

Figure 2b shows the number of flights and average increases in airborne time and ground distance between the rerouting (circumpolar) and baseline (cross-polar) cases. The increase

Table 3 Global and 2006 annual aircraft gas and aerosol emissions from the baseline and rerouting inventories

Species (emission units)	Baseline	Rerouting	% Difference
[a]CO (Tg)	0.67608	0.67622	+0.0258
[a]THC (Tg-CH_4)	0.097586	0.097608	+0.0225
[a]NO_x (Tg-NO_2)	2.6671	2.6690	+0.0710
[b]H_2O (Tg)	231.56	231.69	+0.0561
[b]CO_2 (Tg-CO_2)	594.22	594.56	+0.0561
[b]SO_x (Tg-SO_2)	0.22121	0.22134	+0.0561
[c]BC (Tg-C)-exhaust	0.015668	0.015655	+0.0548–0.0830
[d]BC (Tg-C)-tire & brake	0.004065	0.004065	0
[c]POM (Tg-POM)	0.0080529	0.0080526	+0.0619–0.0037
[b]S(VI) (Tg-H_2SO_4)	0.0069129	0.0069167	+0.0561

[a] Emission determined from flight mode emission factors applied to each segment of each flight in raw Volpe inventory

[b] Emission determined from constant emission factors applied to each segment of each flight: 1231 g-H_2O/kg-fuel; 3159 g-CO_2/kg-fuel; 1.176 g-SO_2/kg-fuel; 0.03675 g-H_2SO_4-PM/kg-fuel

[c] Emissions determined from flight mode emission factors in Table 4 applied to each segment of each flight

[d] Tire and brake emissions of BC=130 g/landing and 0.03 g/landing, respectively (Whitefield et al. 2008), for each of the 31.26 million flights in 2006. Almost all such emissions occur in particles >2.5 μm diameter (*ibid.*)

in airborne time varied greatly by O-D region. The routes with the most time above the Arctic Circle increased airborne time and ground distance most.

The 4-D flight paths of each of the 40,399 rerouted cross-polar flights replaced the original flights in the baseline global 2006 emission inventory. Table 2 summarizes the monthly and annual fuel use for the baseline and rerouting inventories, globally and above the Arctic Circle. Rerouting emissions slightly increased global fuel use by +0.056 % and fuel use for flights that previously flew over the Arctic Circle but now flew around the Circle by +7.52 %. However,

Table 4 Emission factors for BC and POM (g/kg-fuel), mass ratio of NO_2/NO_x emissions, geometric mean number diameters in the volatile-particle mode (GMND-VP) and BC emission mode (GMND-BC), and fraction of POM that is soluble (f_{solub}) as a function of flight status mode. Particles from both modes were discretized into size bins for use in the model

Flight status mode[a]	BC [b]	POM [b]	g-NO_2/g-NO_x [c]	GMND-VP [d]	GMND-BC [e]	f_{solub} [f]
Taxi out	0.1	0.06	0.91	5.0	41.35	0.2
Takeoff ground roll	0.25	0.08	0.08	5.0	41.35	0.1
Takeoff airborne	0.25	0.08	0.08	5.0	41.35	0.1
Terminal climb	0.25	0.08	0.087	5.0	41.35	0.1
En route climb	0.25	0.08	0.087	5.0	41.35	0.1
Cruise	0.03	0.03	0.092	4.7	32.82	0.8
En route descent	0.03	0.03	0.15	4.7	32.82	0.8
Approach	0.03	0.03	0.15	4.7	32.82	0.8
Landing ground roll	0.03	0.03	0.15	4.7	32.82	0.8
Reverse-thrust landing ground roll	0.2	0.08	0.15	5.0	41.35	0.1
Taxi in	0.1	0.06	0.91	5.0	41.35	0.2

[a] Taxi out: start and end altitude =0 ft. above ground level (AGL)

Takeoff ground roll: Start altitude =0 ft. AGL; end altitude >0 ft. AGL; thrust = max takeoff

Takeoff airborne: Start and end altitude >0 ft. AGL; thrust = max takeoff

Terminal climb: Start altitude >0 ft. AGL; end altitude =10,000 ft. AGL; thrust = max climb

En route climb: Start altitude =10,000 ft. AGL; end altitude = cruise altitude; thrust = max climb

Cruise: Start and end altitude = cruise altitude

En route descent: Start altitude = cruise altitude; end altitude =10,000 ft. AGL

Approach: Start altitude =10,000 ft. AGL; end altitude =0 ft. AGL

Landing ground roll: Start and end altitude = 0 ft. AGL

Reverse thrust landing ground roll: Start and end altitude =0 ft. AGL

Taxi in: Start and end altitude = 0 ft. AGL

[b] Whitefield et al. (2008) as a function of thrust: 7 % thrust (idle, taxi), 0.0033–0.27 g-PM/kg-fuel; 15–40 % thrust (approach, cruise), 0.0013–0.07 g-PM/kg-fuel; 60–80 % thrust: 0.03–0.08 g-PM/kg-fuel; ≥85 % thrust (takeoff, climb): 0.1–0.33 g-PM/kg-fuel; high thrust, mostly nonvolatile BC; low thrust, more volatile (POM)

[c] Wood et al. (2008); values estimated as a function of thrust

[d] Figure 2 of Petzold et al. (1999) indicates a GMND of the volatile mode of 4–5 nm and a geometric standard deviation =1.5. BC can enter particles only >14 nm in diameter, the size of the smallest BC spherules

[e] Below 1 km, GMND =41.35 nm; above 1 km, GMND = 32.82 nm. In both cases, geometric standard deviation =1.6

[f] Whitefield et al. (2008) as a function of thrust: low thrust, 20 % of POM is insoluble lubricating oil, thus soluble portion of POM is 80 %; high thrust, 80–90 % of POM is insoluble lubricating oil, thus soluble portion of POM is 10–20 %

The smallest emitted aircraft particles were assumed to consist of sulfate and POM

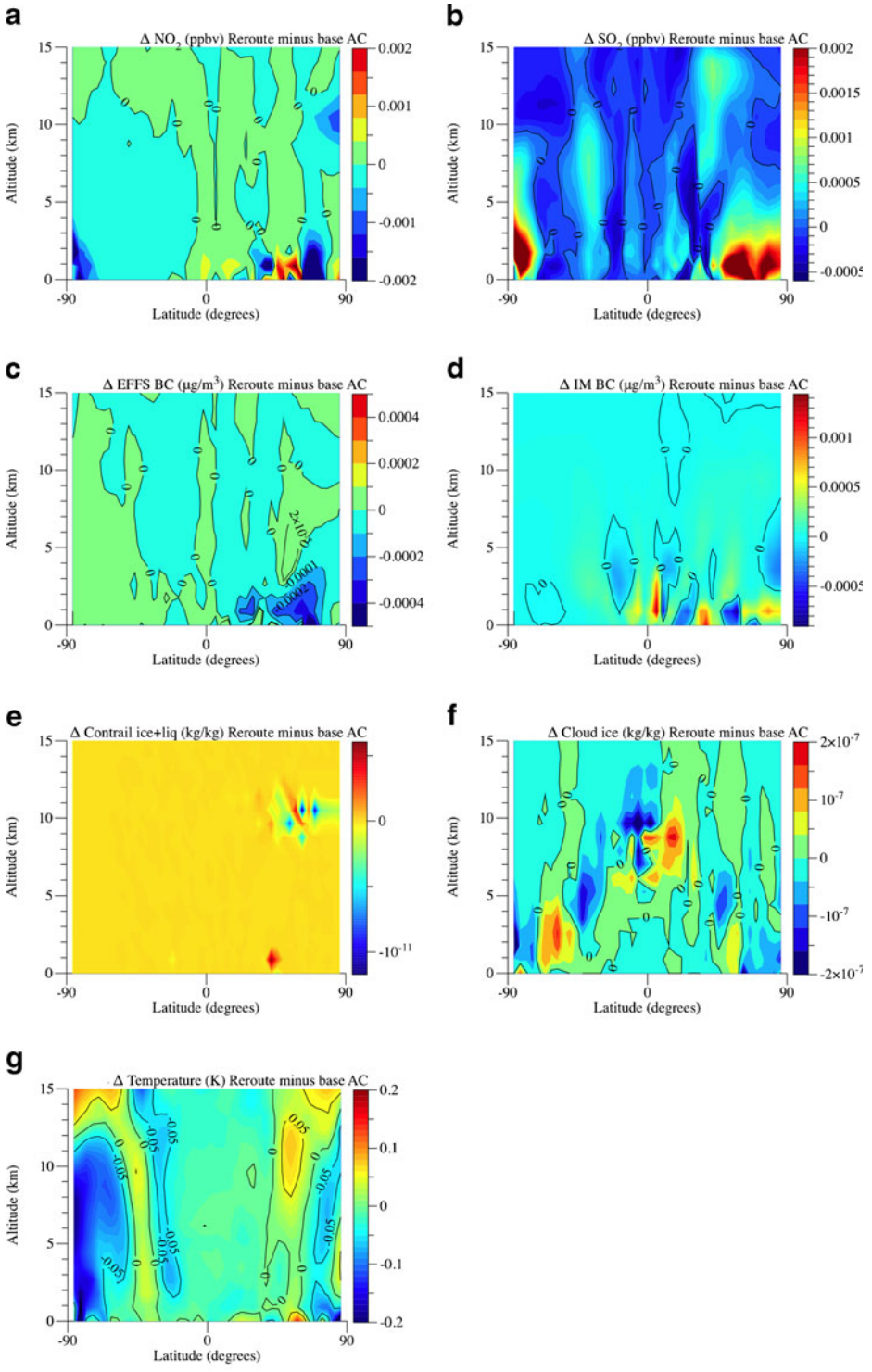
a
Δ NO2 (ppbv) Reroute minus base AC
b
Δ SO2 (ppbv) Reroute minus base AC
c
Δ EFFS BC (μg/m3) Reroute minus base AC
d
Δ IM BC (μg/m3) Reroute minus base AC
e
Δ Contrail ice+liq (kg/kg) Reroute minus base AC
f
Δ Cloud ice (kg/kg) Reroute minus base AC
g
Δ Temperature (K) Reroute minus base AC
Altitude (km)
Latitude (degrees)

such emissions were shifted to latitudes (60–66.56 N) of 3–4 times higher precipitation (e.g., Jacobson and Streets 2009, Fig. 3) and greater vertical instability (Whitt et al. 2011) than above the Arctic Circle. Thus, they were wet-removed more readily. Rerouting also dramatically decreased fuel use above the Arctic Circle itself by 82.6 %. Some emissions above the Arctic Circle still occurred since not all flights were rerouted, as discussed previously.

Although the rerouting inventory increased global fuel use by 0.056 %, it increased CO and THC emissions by only 0.026 % and 0.023 %, respectively (Table 3). The reason is that, whereas fuel use below 3000 ft (914.4 m) during the landing and takeoff (LTO) cycle comprised approximately 10.7 % of all-altitude fuel burn, LTO CO and THC emissions represented 40.4 % and 44.9 %, respectively, of all-altitude emissions. Since rerouting affected primarily cruise-altitude emissions but not LTO emissions, CO and THC emission changes due to rerouting were much lower than were emission changes due to other species (Table 3), which were emitted relatively proportionally to fuel burn in and above the LTO region. Table 4 shows emission factors of BC and POM, the mass ratio of NO_2/NO_x, size distribution parameters, and the solubility of organic matter assumed here as a function of flight status mode in the model.

Jacobson et al. (2011) describe the implementation of aircraft emissions into the model. Briefly, time-dependent emission data from each flight in the raw inventories were provided in segments, and each segment was placed into a unique subgrid plume in each grid cell of the model where all or part of the segment resided. Each of many subgrid plume in each cell was tracked over time during its expansion until the plume merged to the grid scale.

4 Simulations and results

Two 22-year simulations were run, one with the baseline and the other with the rerouting emission inventory. The simulations took over a year of computer time and were stopped after substantial convergence of temperature and short-lived pollutants. Simulations were initialized with 1 °×1 ° reanalysis fields for 12 GMT, January 1, 2006 (GFS 2007) and used a 30-s dynamics time step. Aircraft emissions for 2006 were repeated annually. After initialization, the model was prognostic (no data assimilation or nudging).

Figure 3 shows annual CO_2-C emissions globally and over the Arctic Circle in the baseline and rerouting cases. Although Arctic-circle CO_2-C emissions represented only 0.742 % of the total global CO_2-C mass emissions from aircraft in the baseline case, they were 17.8 % of the globally averaged CO_2-C emission rate per unit surface area of Earth since Arctic Circle area is small relative to Earth's area. Thus, the CO_2-C emission density over the Arctic was relatively high.

The reduction in Arctic-Circle emissions due to rerouting decreased ambient 9–11 km mixing ratios over the Arctic of NO, SO_2, EFFS BC, IM BC (Fig. 4a–d), POM (similar to Fig. 4d), and S(VI) (Similar to Fig. 4d). Whereas, Arctic PM emission reductions reduced PM concentrations in the EFFS aerosol distribution since that is the distribution into which aircraft PM was emitted into, they also decreased PM in the IM distribution. The reason is that EFFS particles internally mix over time to become IM particles, so reducing EFFS particle mass also reduces IM particle mass. Although EFFS BC emissions increased outside the Arctic Circle due to

◀ **Fig. 4** Horizontal difference plots for several parameters from 22-year global simulations that used the 2006 rerouting aircraft emission inventory ("reroute") each year versus the baseline 2006 emission inventory each year ("base AC")

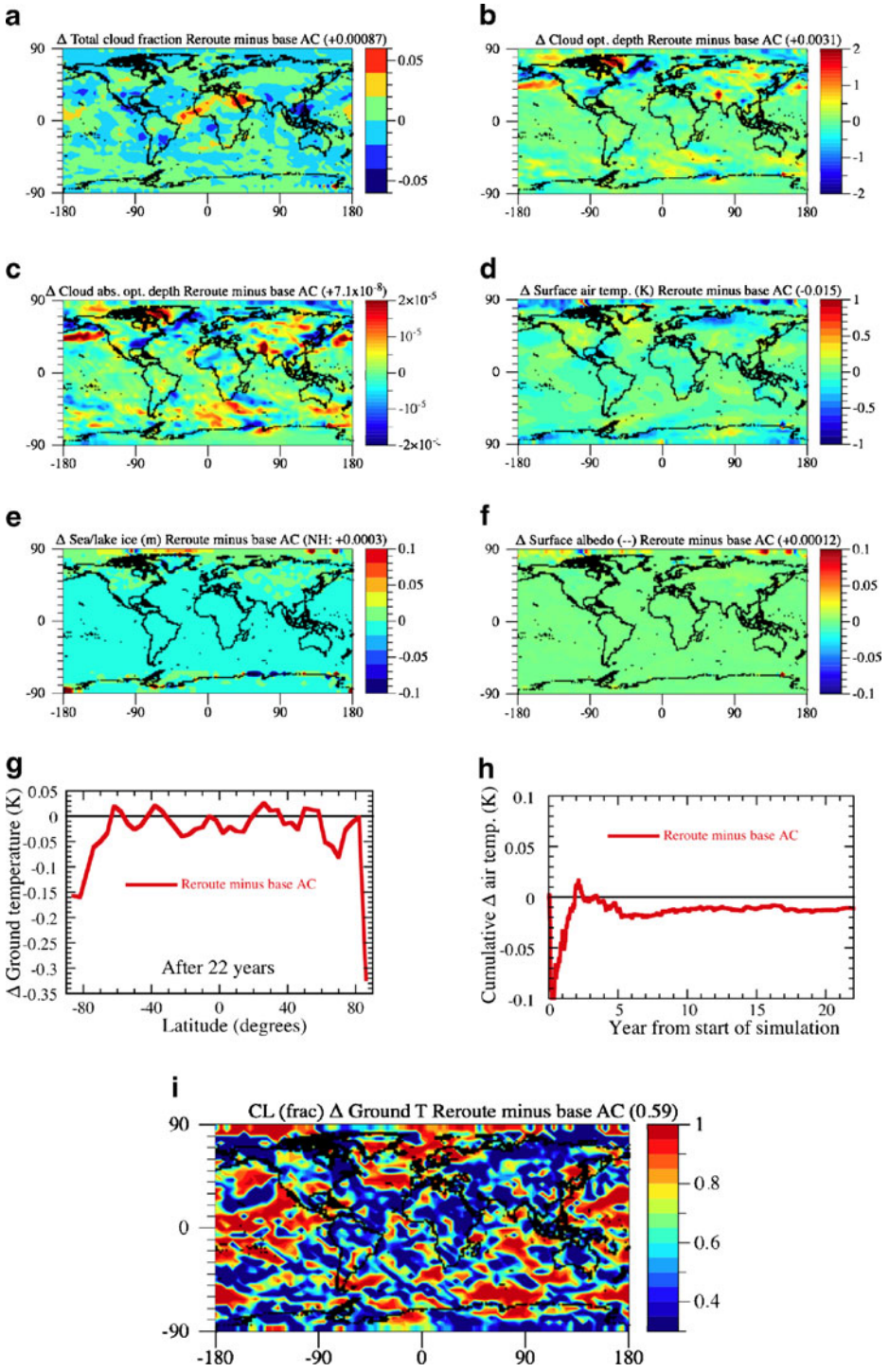
a
Δ Total cloud fraction Reroute minus base AC (+0.00087)
b
Δ Cloud opt. depth Reroute minus base AC (+0.0031)
c
Δ Cloud abs. opt. depth Reroute minus base AC (+7.1x10-8)
d
Δ Surface air temp. (K) Reroute minus base AC (-0.015)
e
Δ Sea/lake ice (m) Reroute minus base AC (NH: +0.0003)
f
Δ Surface albedo (--) Reroute minus base AC (+0.00012)
g
Δ Ground temperature (K)
Reroute minus base AC
After 22 years
Latitude (degrees)
h
Cumulative Δ air temp. (K)
Reroute minus base AC
Year from start of simulation
i
CL (frac) Δ Ground T Reroute minus base AC (0.59)

rerouting, much of such additional emissions were rained out due to higher precipitation there than over the Arctic. Due to the time lag between emissions and internal mixing, IM distribution changes also occurred over a larger atmospheric volume than EFFS distribution changes. In fact, IM BC decreased the most between 2 and 8 km altitude (Fig. 4d). Slight IM BC increases occurred from 9 to 11 km over the Arctic Circle due to the transport of enhanced BC from just outside the Arctic Circle into it.

The reduction in aircraft exhaust over the Arctic Circle reduced contrail water (Fig. 4e). Because fuel burn increased just outside the Arctic Circle due to rerouting, contrail water increased there. Most changes in contrails occurred between 9 and 11 km.

The reduction in internally-mixed BC-, POM-, and S(VI)-containing aerosol particles reduced ice cloud water (Fig. 4f), total cloud fraction (Fig. 5a), and cloud optical depth (Fig. 5b) over much of the Arctic Circle due to reduced indirect effects of aerosols on clouds. The reductions in cloudiness and BC concentration reduced cloud absorption optical depths over much of the Arctic (Fig. 5c).

The reduction in absorption of solar and thermal-IR radiation by BC in clouds and aerosols over the Arctic, in turn, helped to decrease near-surface and aloft temperatures (Figs. 4g, 5d). The reduction in cloudiness (both contrail and background) and the local CO_2 reduction of up to 17 g/m^2 over the low-sunlight Arctic also increased outgoing thermal-IR radiation, contributing to surface cooling there. The maximum surface temperature decrease due to rerouting, 0.3 K, occurred at 86 N. Another peak decrease occurred at 70 N (Fig. 5g). Comparatively, surface temperature increases averaged above the Arctic Circle due to fossil-fuel plus biofuel soot from all sources worldwide were modeled as >1 K (Jacobson 2010). Decreases in soot-BC in snow due to reduced northern Eurasian emissions since 1989 (Hirdman et al. 2010) may be alleviating some of this warming.

Arctic temperature decreases extended in most locations up to 13 km (Fig. 4g). Temperatures increased just outside the Arctic Circle, where aircraft emissions increased due to an increase in circumpolar flights from rerouting. Due mostly to Arctic cooling, global surface temperatures decreased by 0.015 K (Fig. 5d), or 1.75–2 % of net global warming (0.7–0.8 K) to date. The global temperature changes due to rerouting were relatively constant between years 5 and 22 (Fig. 5h).

The top-of-the-atmosphere global irradiance change was −0.03 W/m^2, with values up to −3 W/m^2 over the Arctic. The resulting global climate sensitivity due to rerouting was 0.5 K/W/m^2, close to values for other forcing agents from numerous studies.

The decrease in surface temperatures due to rerouting increased Arctic sea ice thickness (Fig. 5e) and albedo (Fig. 5f). Any increase in sea ice will delay the positive feedback that otherwise results in faster global warming as well as improve the survivability of polar bears (e.g., Stirling and Parkinson 2006).

◀ **Fig. 5** **a–f** Zonally-averaged latitude-altitude difference plots for several parameters from 22-year global simulations with the 2006 rerouting aircraft emission inventory ("reroute") each year versus the 2006 baseline inventory ("base AC"). **g** Zonally-averaged ground temperature difference between the rerouting and baseline cases. **h** Cumulative globally-averaged surface air temperature change during the simulation. This is the simulation- and globally-averaged air temperature change averaged between the beginning of the simulation and any time during the simulation. The cumulative value at the last time is the simulation-averaged value. **i** Confidence level, calculated from a non-directional *t*-test, of the modeled four-year ground temperature difference between the rerouting and baseline simulations relative to six simulations randomly perturbed from the baseline simulation

5 Statistical significance of results

To check the statistical significance of the rerouting versus the baseline simulations relative to natural variations in the model arising from the fact that atmospheric dynamical processes are deterministically chaotic, six additional simulations were run for 4 years in which the initial value of one parameter in the baseline simulation was varied randomly at one location. Four years was justified because significance test results for 4 years were similar to those for 2 and 3 years.

Ground temperature differences between the rerouting and baseline cases were compared with the standard deviation among the random-perturbation simulations within each model surface grid cell with a non-directional *t*-test similarly (e.g., Chervin and Schneider 1976). Figure 5i shows the resulting confidence level (CL) of the statistical significance for each model surface grid cell. CLs of 95 % or higher suggest strong statistical significance. Results for about 16 % of the Earth were significant to the 95 % CL; results for 30 % were significant to the 85 % CL. However, CLs above 80 N were high, particularly where modeled temperature changes were greatest (Fig. 5d) and where the statistical significance of the results here are most relevant.

6 Costs and policy implications

The average cost of U.S. jet fuel in 2006 was $1.93/gal (BTS 2011). Jet fuel density at 15°C ranges from 690 kg/m^3 for BP Avgas 80 to 787 kg/m^3 for Kerosene type BP Jet TS-1 to 804 kg/m^3 for Kerosene type BP Jet A-1. Assuming for simplicity a density of 787 kg/m^3 and 264.17 U.S. gallons/m^3, the annual 2006 cost of fuel in the baseline case for all flights worldwide and the segments of flights above the Arctic Circle were ~$122 billion/yr and $904 million/yr, respectively. With 0.056 % higher fuel use, the 2006 fuel cost due to rerouting worldwide would be ~$68 million/yr, higher.

Additional non-fuel rerouting-related operational costs include variable costs for crew and maintenance, which increase with increasing airborne time. These costs were ~$31 million/yr based on Form 41 actual cost data for 2006, submitted by U.S. carriers (Bureau of Transportation Statistics. www.bts.gov). We assumed no additional fixed costs per flight associated with aircraft operation, such as aircraft rental, depreciation, and insurance, since we assumed no decrease in the number of flights scheduled for aircraft that flew longer routes during rerouting. In sum, the overall 2006 fuel plus operational cost of rerouting is estimated at ~$99 million/yr.

This increase in fuel and operational costs must be balanced against the environmental and human health cost benefits of rerouting. Such benefits result from reducing global temperatures. The reduction in global near-surface temperatures due to rerouting here was 0.015 K over the 22-year simulations. One set of cost estimates for global warming (in 2006 U.S. dollars) to the U.S. alone is $271 billion/yr by 2025, $506 billion/yr by 2050, $961 billion/yr by 2075, and $1.9 trillion/yr by 2100 (Ackerman et al. 2008). That analysis accounted for severe-storm damage, real estate loss, energy-sector costs, and water costs alone. The largest of these costs was water costs. It did not account for mortality and illness increases due to heat stress, influenza, malaria, and air pollution or forest-fire increases; thus, it may be conservative. If rerouting reduces global warming by 1.75–2 %, as found here, 2025 global warming damage may decrease by $4.7–5.4 billion/yr in the U.S. alone, or 47–55 times the worldwide fuel plus operational cost of rerouting.

Although the 0.056 % CO_2 emission increase due to rerouting may dampen the benefit of rerouting decades beyond the 22 years simulated here, rerouting delays the elimination of Arctic sea ice, which may otherwise occur within 2–3 decades. Since some of the cooling

due to rerouting was due to reduction in solar absorption by BC, an alternative to complete rerouting may be partial rerouting by allowing cross-polar flights during only polar night.

The longer-term effects of CO_2 emissions due to aircraft also need to be addressed, possibly by conversion to more efficient aircraft and, ultimately, cryogenic hydrogen fuel for aircraft, where the hydrogen is produce by electrolysis from a carbon-free electricity source. Such aircraft would need to be more voluminous but less massive than current aircraft, resulting in similar overall efficiencies (Coenen 2009; Janic 2008).

7 Conclusions

This paper examined the effects on Arctic and global climate of rerouting most cross-polar aircraft flights around the Arctic Circle. Baseline and rerouting emission inventories for 2006 were developed that accounted for the complete track of each individual commercial flight worldwide. The rerouting inventory rerouted most cross-polar flights around the Arctic Circle. Rerouting flights increased fuel use and total pollution emissions by 0.056 %, but most such emissions were removed faster by wet deposition because they were now over latitudes of greater precipitation and lesser stability. Rerouting also reduced emissions within the Arctic Circle by 83 % and delayed the transport of pollutants from outside to within the Arctic Circle. The reduction in pollutants, particularly black carbon, in the Arctic decreased Arctic and global temperatures and Arctic sea ice loss over two decades. Although the slight CO_2 emission increase due to rerouting may dampen the benefit of rerouting over many more decades, rerouting or partial rerouting (allowing cross-polar flights during polar night only) should delay the elimination of Arctic sea ice, which is otherwise expected in 2–3 decades. The worldwide fuel plus operational cost of rerouting is estimated at ~ U.S. $99 million/yr, 47–55 times less than one estimate of the 2025 cost benefit to the U.S. alone resulting from reducing Arctic and global temperatures due to rerouting.

Acknowledgments Support for Stanford under PARTNER/FAA DTFAWA-05-D=0006. Support for MITRE/CAASD under FAA DTFA01-01-C-00001. Any opinions, findings, conclusions, or recommendations do not necessarily reflect PARTNER or FAA views. We thank David Senzig and Gary Baker at Volpe for help with emission data and Ehsan Esmaeilzadeh and Andy Meyers at MITRE/CAASD for help with rerouting analysis.

References

Ackerman F, Stanton EA Hope C, Alberth S, Fisher J Biewald B (2008) The cost of climate change. www.nrdc.org/globalwarming/cost/cost.pdf. Accessed July 21, 2011

BTS (2011) Airline fuel cost and consumption (US. Carriers–scheduled) Jan 2000-Apr 2011. http://www.transtats.bts.gov/fuel.asp. Accessed Oct 1, 2011

Chervin RM, Schneider SH (1976) On determining the statistical significance of climate experiments with general circulation models. J Atmos Sci 33:405–412

Coenen RM (2009) A proposal to convert air transport to clean hydrogen (CATCH). Int J Hyd Energy 34:8451–8453

Cooper WW, Esmaeilzadeh E, Meyers A, Mohleji N (2011) Trans-Arctic Route Analysis. MITRE Technical report 100024, McLean, Virginia, August 2011

Corbett JJ, Lack DA, Winebrake JJ, Harder S, Silberman JA, Gold M (2010) Arctic shipping emissions inventories and future scenarios. Atmos Chem Phys 10:9689–9704

GFS (2007) 1 °×1 ° reanalysis fields. http://nomads.ncdc.noaa.gov/data/gfs-avn-hi/. Accessed January 20 2008

Hegg DA, Warren SG, Grenfell TC, Doherty SJ, Larson TV, Clarke AD (2009) Source attribution of black carbon in Arctic snow. Environ Sci Technol 43:4016–4021

Hirdman D, Burkhart JF, Sodemann H, Eckhardt S, Jefferson A, Quinn PK, Sharma S, Strom J, Stohl A (2010) Long-term trends of black carbon and sulphate aerosol in the Arctic: changes in atmospheric transport and source region emissions. Atmos Chem Phys 10:9351–9368

Holland MM, Bitz CM, Tremblay B (2006) Future abrupt reductions in the summer Arctic sea ice. Geophys Res Lett 33:L23503. doi:10.1029/2006GL028024

Jacobson MZ (2010) Short-term effects of controlling fossil-fuel soot, biofuel soot and gases, and methane on climate, Arctic ice, and air pollution health. J Geophys Res 115:D14209. doi:10.1029/2009JD013795

Jacobson MZ, Streets DG (2009) Influence of future anthropogenic emissions on climate, natural emissions, and air quality. J Geophys Res 114:D08118. doi:1029/2008JD011476

Jacobson MZ, Wilkerson JT, Naiman AD, Lele SK (2011) The effects of aircraft on climate and pollution. Part I: numerical methods for treating the subgrid evolution of discrete size- and composition-resolved contrails from all commercial flights worldwide. J Comp Phys 230:5115–5132. doi:10.1016/j.jcp.2011.03.031

Janic M (2008) The potential of liquid hydrogen for the future 'carbon-neutral' air transport system. Transport Res D 13:428–435

Koch D, Hansen J (2005) Distant origins of Arctic black carbon: a Goddard Institute for Space Studies model-E experiment. J Geophys Res 110:D04204. doi:10.1029/2004JD005296

Liu J, Fan S, Horowitz LW, Levy H II (2011) Evaluation of factors controlling long-range transport of black carbon to the Arctic. J Geophys Res 116:D04307. doi:10.1029/2010JD015145

Matsui H et al (2011) Seasonal variation of the transport of black carbon aerosol from the Asian continent to the Arctic during the ARCTAS aircraft campaign. J Geophys Res 116:D05202. doi:10.1029/2010JD015067

Naiman AD, Lele SK, Wilkerson JT, Jacobson MZ (2010) Parameterization of subgrid aircraft emission plumes for use in large-scale atmospheric simulations. Atmos Chem Phys 10:2551–2560

NCEP/NCAR (2009) Reanalysis. www.esrl.noaa.gov/psd/data/gridded/data.ncep.reanalysis.html. Accessed Aug 26, 2011

NSIDC (2011) Arctic Sea Ice News and Analysis. http://nsidc.org/arcticseaicenews/. Accessed Sep 15, 2011

Petzold A, Dopelheuer A, Brock C, Schroder F (1999) In situ observations and model calculations of black carbon emission by aircraft at cruise altitude. J Geophys Res 104:22,171–22,181

Rahn KA, McCaffrey RJ (1980) On the origin and transport of the winter arctic aerosol. Ann N Y Acad Sci 338:486–503

Senzig DA, Baker GM, Balasubramanian SN (2010) Environmental modeling of trans-Arctic and re-routed flights. DOT-VNTSC-FAA-10-04, http://ntl.bts.gov/lib/33000/33500/33556/Transarctic_and_Rerouted_Flights_1_.pdf. Accessed Aug. 8, 2011

Stirling I, Parkinson CL (2006) Possible effects of climate warming on selected populations of polar bears (Ursus maritimus) in the Canadian Arctic. Arctic 59:261–275

Vinnikov KY, Robock A, Stouffer RJ, Walsh JE, Parkinson CL, Cavalieri DJ, Mitchell JFB, Garrett D, Zakharov VF (1999) Global warming and Northern Hemisphere sea ice extent. Science 286:1934–1937

Whitefield PD et al (2008) Summarizing and interpreting aircraft gaseous and particulate emissions data. Aircraft Cooperative Research Program, Report 9, Transportation Research Board, Washington DC

Whitt DB, Wilkerson JT, Jacobson MZ, Naiman AD, Lele SK (2011) Vertical mixing of commercial aviation emissions from cruise altitude to the surface. J Geophys Res 116:D14109. doi:1029/2010JD015532

Wilkerson JT, Jacobson MZ, Malwitz A, Balasubramanian S, Wayson R, Fleming G, Naiman AD, Lele SK (2010) Analysis of emission data from global commercial aviation: 2004 and 2006. Atmos Chem Phys 10:6391–6408

Winton M (2006) Does the Arctic sea ice have a tipping point? Geophys Res Lett 33:L23504. doi:10.1029/2006GL028017

Wood EC, Herdon SC, Timko MT, Yelvington PE, Miake-Lye RC (2008) Speciation and chemical evolution of nitrogen oxides in aircraft exhaust near airports. Environ Sci Technol 42:1884–1891